Osteocyte calcium signals encode strain magnitude and loading frequency in vivo

Karl J. Lewis[a], Dorra Frikha-Benayed[a], Joyce Louie[a], Samuel Stephen[a], David C. Spray[b], Mia M. Thi[c], Zeynep Seref-Ferlengez[c], Robert J. Majeska[a], Sheldon Weinbaum[a,1], and Mitchell B. Schaffler[a,1]

[a]Department of Biomedical Engineering, City College of New York, New York, NY 10031; [b]Department of Neuroscience, Albert Einstein College of Medicine, Bronx, NY 10461; and [c]Department of Orthopaedic Surgery, Albert Einstein College of Medicine, Bronx, NY 10461

Contributed by Sheldon Weinbaum, September 14, 2017 (sent for review May 11, 2017; reviewed by Tamara Alliston and Henry J. Donahue)

Osteocytes are considered to be the major mechanosensory cells of bone, but how osteocytes in vivo process, perceive, and respond to mechanical loading remains poorly understood. Intracellular calcium (Ca^{2+}) signaling resulting from mechanical stimulation has been widely studied in osteocytes in vitro and in bone explants, but has yet to be examined in vivo. This is achieved herein by using a three-point bending device which is capable of delivering well-defined mechanical loads to metatarsal bones of living mice while simultaneously monitoring the intracellular Ca^{2+} responses of individual osteocytes by using a genetically encoded fluorescent Ca^{2+} indicator. Osteocyte responses are imaged by using multiphoton fluorescence microscopy. We investigated the in vivo responses of osteocytes to strains ranging from 250 to 3,000 με and frequencies from 0.5 to 2 Hz, which are characteristic of physiological conditions reported for bone. At all loading frequencies examined, the number of responding osteocytes increased strongly with applied strain magnitude. However, Ca^{2+} intensity within responding osteocytes did not change significantly with physiological loading magnitudes. Our studies offer a glimpse into how these critical bone cells respond to mechanical load in vivo, as well as provide a technique to determine how the cells encode magnitude and frequency of loading.

osteocytes | calcium signaling | mechanotransduction | in vivo loading | bone

Bone has a remarkable ability to sense mechanical load and adapt its structure in response. This mechanical adaptation ability is so prominent for bone that it was among the first organ systems to be recognized in this regard; indeed, the word "orthopedics," first coined in the mid-1700s, derives from straightening the bones of children. The ability of bone to adapt its structure is essential for growing a skeleton appropriate to its mechanical demands and for maintaining the integrity of that skeleton throughout life. Osteoblasts and osteoclasts are the effector cells that carry out bone formation and resorption (respectively), and their dysfunction leads to growth defects and osteoporosis. However, it is increasingly recognized that osteocytes, buried within the bone matrix, are the major local orchestrators of diverse functions in bone. They produce soluble signaling factors that regulate both bone formation and resorption, local mineralization, and also calcium (Ca^{2+}) and phosphate transport at the bone matrix level. They also function as endocrine cells, producing factors such as FGF23, that have an impact on renal functions. Among the most essential functions of osteocytes is sensing mechanical load to which bone is subjected and transducing this load into downstream signals, which regulate osteoblasts and osteoclasts.

Osteocytes in situ exist in a complex, 3D, highly interconnected array. Osteocyte cell bodies and processes reside in spaces (lacunae and canaliculi, respectively) within bone matrix and are surrounded in these spaces by a fluid-gel layer that fills the lacunar-canalicular space (LCS). This fluid layer, which moves when bones are mechanically loaded, transmits mechanical forces and determines much of how osteocytes experience their environment. It also accounts for solute transport to and from osteocytes, including metabolites as well as key osteocyte-produced signaling molecules such as sclerostin, RANKL, and OPG. Osteocyte expression of these key signaling molecules is sensitive to changes in mechanical load as well as other stimuli that initiate bone remodeling, such as changes in gonadal steroids and local tissue microdamage (1–4).

Mechanical loads at the bone tissue level are translated to fluid flow in the LCS (5–7). Indeed, a growing body of evidence indicates that fluid flow through the LCS dominates the local mechanical input to osteocytes in situ (8–11). Mechanical stimulation of osteocytes increases cytoplasmic Ca^{2+}, a ubiquitous response to both mechanical and biochemical stimuli (12–15). In particular, Thi et al. demonstrated with cells that fluid forces acting on the $\alpha_v\beta_3$ integrin adhesion sites on osteocyte cell processes in vitro triggered Ca^{2+} responses that spread toward the cell body and then initiated a typical whole-cell Ca^{2+} signaling response like that seen in other cells (16). Finally, most studies of osteocyte Ca^{2+} signaling have been conducted either in 2D cell cultures or in explanted bones (10, 17), which have limitations. Cell cultures lack the LCS and attendant localized tissue architecture and fluid flow, while bone explants are subject to postmortem tissue changes, as well as fluid pressure loss in the LCS resulting from loss of in vivo vascular pressure (8, 18, 19).

In the present studies, we report an in vivo approach to explore osteocyte Ca^{2+} signaling in whole bone where the cells can be individually imaged during mechanical loading. We generated a mouse model with an osteocyte-targeted genetically encoded Ca^{2+} indicator (GECI) to study Ca^{2+} signaling in osteocytes in their authentic in vivo environment. We also created a bone loading approach for use in live mice while simultaneously

Significance

Osteocytes are thought to be the major regulator of bone mechanosensation events. However, little is known about how osteocytes in vivo acutely respond to tissue-level mechanical loading. We report here a technique for the direct in vivo observation of osteocyte calcium signaling events with simultaneous whole bone loading. Our results demonstrate that osteocyte populations integrate mechanical signals by altering the number of responding cells and that this effect is dependent on loading frequency.

Author contributions: K.J.L., D.C.S., S.W., and M.B.S. designed research; K.J.L., D.F.-B., M.M.T., and Z.S.-F. performed research; K.J.L., J.L., and S.S. analyzed data; and K.J.L., R.J.M., and M.B.S. wrote the paper.

Reviewers: T.A., University of California, San Francisco; and H.J.D., Virginia Commonwealth University.

The authors declare no conflict of interest.

[1]To whom correspondence may be addressed. Email: weinbaum@ccny.cuny.edu or mschaffler@ccny.cuny.edu.

This article contains supporting information online at www.pnas.org/lookup/suppl/doi:10.1073/pnas.1707863114/-/DCSupplemental.

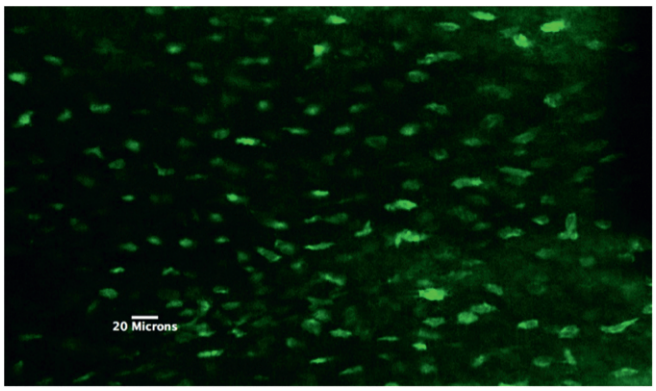

Fig. 1. Multiphoton z-stack image of OtGP3 MT3 osteocytes in vivo. Note that all cells in the field of view exhibit GCaMP3 signal, indicating highly efficient expression in osteocytes.

observing the intracellular Ca^{2+} responses of individual osteocytes with multiphoton microscopy (MPM). We report how Ca^{2+} signaling of osteocytes in vivo, both individually and as networks, responds to mechanical loading. We used this approach to test the hypothesis that encoding of mechanical strain and frequency information by osteocytes in vivo is based on recruitment of responding cells (i.e., numerical encoding) rather than on graded Ca^{2+} responses by individual cells.

Results

Osteocyte GCaMP3 Expression. Mice expressing the osteocyte-targeted GECI GCaMP3, which are here termed OtGP3, were created. Baseline GCaMP3 fluorescence was visible in osteocytes throughout the diaphyseal cortex (Fig. 1). In pilot studies, we found that >95% of osteocytes in OtGP3 mice exhibited detectable fluorescence. Fluorescence intensity level varied among cells, and resting osteocytes exhibited low-level fluctuations in Ca^{2+} fluorescence intensity (Fig. 2).

Bone Structure in OtGP3 Mice. Our studies used the third metatarsal (MT3) of the mouse foot. Previous studies in our group demonstrated that this bone is well-suited for direct visualization of cortical bone osteocytes in living animals by using MPM (20). Its tubular geometry lends itself to bending without creating off-axis stresses. MT3 bones from OtGP3 mice had larger cortical bone areas, but slightly lower tissue mineral density than WT bones (Table 1; $P < 0.05$), resulting in similar cross-sectional moduli and diaphyseal bending rigidities.

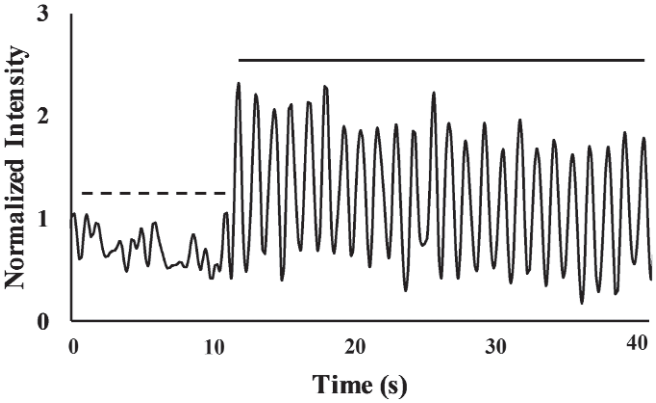

Fig. 2. A representative Ca^{2+} trace for a single osteocyte before (dashed line) and after the start of cyclical loading (solid line) at 1 Hz to 3,000 με. Before mechanical loading, all osteocytes exhibited low-level Ca^{2+} fluctuations. Immediately following the start of mechanical loading, responsive cells showed cyclic increases in Ca^{2+} fluorescence intensity coinciding with the applied loading frequency.

Osteocyte Response to Mechanical Loading in Vivo. We used a custom-designed device to deliver controlled mechanical strains to MT3 bones of living OtGP3 mice while simultaneously monitoring intracellular Ca^{2+} responses with MPM. Ca^{2+} fluorescence in responding cells increased very rapidly, within 200 ms of loading onset (Fig. 2), and oscillations followed the applied loading (Movie S1). Osteocytes were examined in bones loaded cyclically to habitual physiological strain magnitudes [250, 500, 1,000, and 2,000 microstrain(με)] as well as a nonhabitual high strain level (3,000 με). Loading frequency effects were examined as well (0.5, 1, or 2 Hz; $n = 6$ animals per loading frequency group).

Once activated, Ca^{2+} response intensity remained consistent for each osteocyte for loading up to 2,000 με. Osteocyte Ca^{2+} intensity increased only with loading to 3,000 με (Fig. 3; $P < 0.05$, ANOVA). In contrast, the number of Ca^{2+} responding osteocytes increased markedly with increasing strain magnitude for all loading frequencies tested (Fig. 4). At 0.5- and 1-Hz loading, the load–response curves (i.e., relationship between responding osteocytes and strain magnitude) were linear ($P < 0.01$). However, osteocyte "recruitment rate" (i.e., the number of responding osteocytes per strain level) was approximately twofold greater at 1- vs. 0.5-Hz loading (0.023 vs. 0.012; $P < 0.001$, analysis of covariance). The load–response curve was fundamentally different at 2 Hz. At this frequency, the number of Ca^{2+} responding osteocytes was near zero for strains of <1,000 με. Above this strain level, osteocyte recruitment increased steeply. The relationship between applied strain levels and responding osteocytes at 2-Hz loading appeared nominally exponential, but was better described by a polynomial relationship ($r^2 = 0.55$ vs. 0.85, respectively). Responding osteocytes were distributed within regions of interest (ROIs) without an apparent spatial pattern. We observed instances in which loading at a given strain level triggered a Ca^{2+} response in one osteocyte, but none in an adjacent osteocyte.

To address the importance of vascular pressure to maintaining the fluid pressure of the LCS, MT3s from an additional group of mice ($n = 3$) were cyclically loaded to a single test strain (2,000 με, 1 Hz) for 60 s while animals were alive and then again at 15 min postmortem (no vascular pressure but cells viable) and 60 min postmortem (severe mitochondrial stress) (20). Amplitude of osteocyte Ca^{2+} response was attenuated markedly at 15 min after death compared with in vivo loading (Fig. 5). These small Ca^{2+} oscillations in response to loading became irregular and did not track the applied loading frequency. The situation further decayed by 60 min.

Discussion

This study provides a report of in vivo osteocyte Ca^{2+} responses to mechanical loading of bone in living animals and provides

Table 1. Bone structure, mineralization, stiffness, and osteocyte density in WT and OtGP3 MT3 bone

Parameter	B6-WT	OtGP3
Bone length, mm	7.75 ± 0.07	7.59 ± 0.14*
Total bone area, mm^2	0.208 ± 0.25 E-2	0.205 ± 0.12 E-2
TMD, g/cm^3	1.15 ± 0.02	1.05 ± 0.02*
Sectional stiffness, N/m	7.58 ± 0.36	7.82 ± 1.03
Ot.N, no./mm^2	491 ± 38	448 ± 39*

Values are mean ± SD. $n = 6$ per group. Ot.N, osteocyte number; TMD, tissue mineral density. *$P < 0.05$.

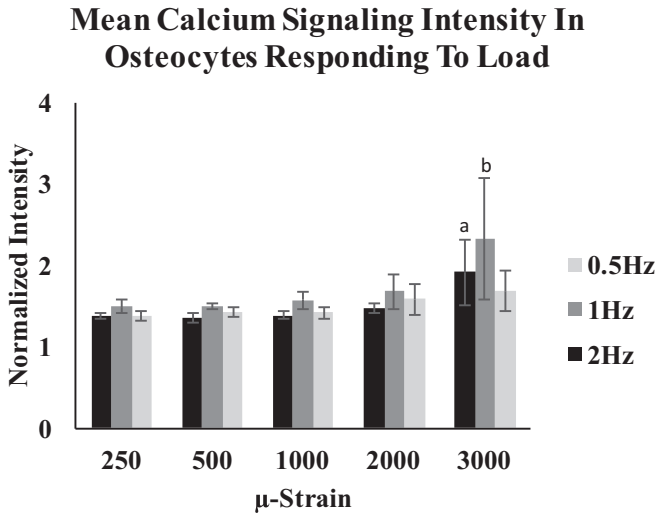

Fig. 3. Intensity of Ca^{2+} signaling per osteocytes was not changed with increasing strain levels up to 2,000 με in all loading rate groups. Increases in Ca^{2+} were noted at 3,000 με. (*a*) $P < 0.05$; 2-Hz loading group; (*b*) $P < 0.05$ 1-Hz loading group. Error bars represent SD, $n = 6$ per group.

critical information about how osteocyte Ca^{2+} transients encode mechanical strain and frequency information that govern bone adaptation to mechanical loading. Using a technology that permitted skeletal loading while simultaneously visualizing fluorescence signals from cortical bone osteocytes, we discovered that osteocytes loaded to strain magnitudes typical of habitual physiological activities respond in an all-or-none fashion (i.e., OFF–ON). In contrast, the number of osteocytes was strongly proportional to applied strain magnitude. Finally, the number of Ca^{2+} responding osteocytes was also strongly influenced by loading frequencies (Fig. 4).

We previously showed that mechanically stimulated Ca^{2+} elevation in osteocytes is triggered through stretch on a cell process integrin attachment that opens channels allowing ATP release (16). This ATP release then causes a Ca^{2+} influx to the osteocyte cell process that in turn triggers the cytoplasmic Ca^{2+} increase observed in the cell body (10, 12, 21, 22). Increased cytoplasmic Ca^{2+} in osteoblast and osteocyte in vitro (23, 24) is a well-established initial response to mechanical stimulation due to a range of mechanical challenges (12, 25–28). Moreover, this Ca^{2+} signaling is implicated in control of expression of PGE2, RANKL, and sclerostin, as well as Wnt, all critical regulators of bone formation and resorption (2, 29–33).

Our findings establish that within the habitual physiological strain range, intensity or magnitude of Ca^{2+} response for individual osteocytes to loading is effectively binary (i.e., all or none). Such "OFF–ON" responses are typical of Ca^{2+} signaling events in a range of cell types and networks, including glia and skeletal and cardiac muscles (34). Interestingly, we observed that some adjacent osteocytes experiencing identical tissue strains appeared to have different thresholds for mechanical activation. Such threshold differences may be intrinsic to the cells and indeed would be expected in a system where cell responses are binary. Alternatively, this could arise from local differences in fluid flow patterns through the LCS, such that adjacent osteocytes do not experience the same local mechanical stimuli (35, 36). Why Ca^{2+} signaling intensity was elevated at 3,000 με remains obscure at this time and requires further investigation. It is worth noting that this high strain is the level at which bone formation switches from controlled lamellar bone apposition to a dysregulated woven bone formation—the "emergency" response system associated with rapid bone proliferation of poorly organized tissue as seen in fracture healing (37, 38). Thus, it seems reasonable to postulate that the change in osteocyte signaling at this high strain level reflects a transition in cell signaling as the bone moves from controlled to proliferative bone-formation response.

The present studies revealed a profound effect of loading frequency on osteocyte recruitment over the range of physiological frequencies examined. Bone formation and remodeling are known to depend strongly on loading rate and frequency, although the physiological basis for frequency effects remains unknown (37, 39–41). There are examples of 'frequency-tuned' excitatory cells in other systems such as the inner ear (42, 43), and osteocytes may be similar. Alternatively, we previously demonstrated that local fluid flow stresses on osteocyte processes in situ can increase sharply over the range of loading frequencies examined in this study, suggesting a way that loading frequency might directly influence what osteocytes experience mechanically (5, 8, 44). This is exemplified in Fig. 6, which shows theoretical predictions for axial strain in the cell membrane at an $\alpha_v\beta_3$ integrin attachment site on an osteocyte process (5). At loading frequencies <2 Hz, there is a roughly linear increase in axial membrane strain as the whole tissue strain is increased from 250 to 1,000 με. This behavior is consistent with our experimental results shown for 0.5 and 1 Hz. In contrast, there is no significant osteocyte response at 2 Hz for this same strain range. Cells are viscoelastic, meaning that they become stiffer as loading rate increases.

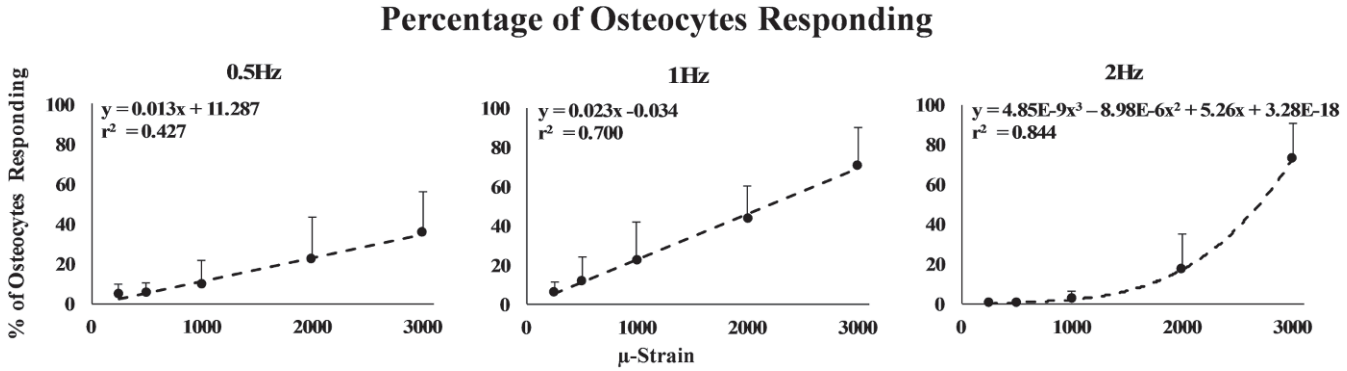

Fig. 4. Shown is the percentage of responding osteocytes as a function of applied strain magnitude for 0.5-, 1-, and 2-Hz loading frequencies. All response curves increased with increasing strain and were effectively linear at 0.5- and 1-Hz loading. The 2-Hz loading response curve was nonlinear. Error bars represent SD. $n = 6$ per frequency group.

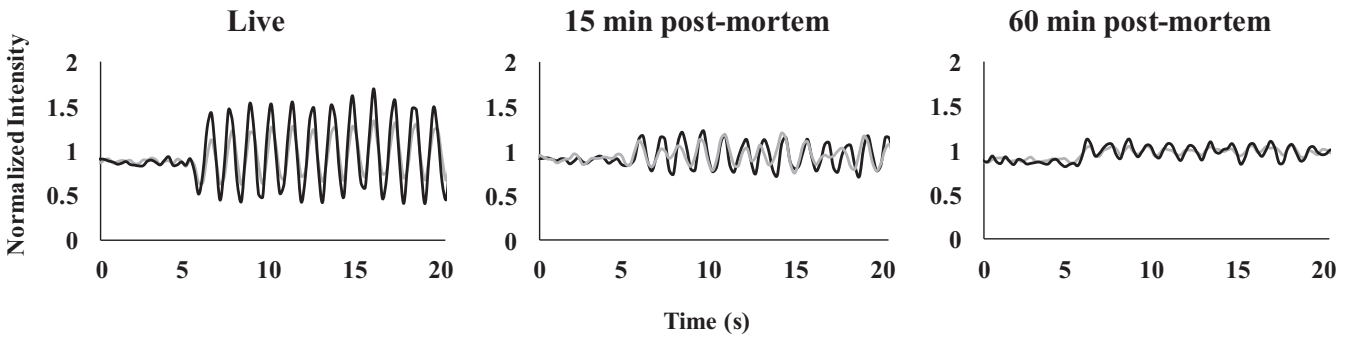

Fig. 5. Typical Ca^{2+} traces for two representative osteocytes before and after the onset of mechanical loading in live bone (*Left*) and at 15 min (*Center*) and 60 min (*Right*) postmortem. Osteocyte Ca^{2+} signal amplitude acutely after death was markedly attenuated compared with in vivo, although the Ca^{2+} signaling still tracked the applied loading frequency. In contrast, at 60 min postmortem, the response of osteocytes to loading was low and irregular, with Ca^{2+} signaling no longer consistent with the applied loading frequency. n = 3 per group.

A stiffer osteocyte would experience reduced membrane strains at mechanotransduction sites; thus, we can reasonably posit that, above some frequency/rate threshold, we would see reduced cell transduction that would be most evident at low loads, as is consistent with the results of this study (45).

A loose association between mechanical loading levels and number of responding osteocytes can be inferred from numerous studies showing strain-dependent changes in expression of molecular markers, including GP6DH activity, prostaglandin synthase, IGF-1, c-fos, and sclerostin (33, 46–48). Thus, an association between the number of Ca^{2+} responding osteocytes and strain magnitude we observed was not unexpected. However, we observed surprisingly high correlations between applied strain magnitudes and the number of Ca^{2+} responding osteocytes. Our results further indicated that osteocyte networks are remarkably precise in their encoding of mechanical frequency input. Tight coupling between input and transducer output signals are characteristic of precise measurement and control systems. Physiological examples include baroreceptors and muscle stretch receptors.

Pereira et al. recently reported a computational model to predict the response of mouse tibiae to anabolic loading based on osteocyte responses (49). They found that normal bone formation rates and predictions of bone adaptation could be achieved only when osteocytes functioned as binary responders (i.e., OFF or ON) above a given threshold strain level, while osteocyte recruitment number varied with load. Bone adaptation was dysregulated when osteocytes were allowed to vary response intensity in a strain-dependent manner, consistent with our experimental results. These results suggest that bone adaptation is regulated by recruiting more osteocytes to the signaling population rather than by modulation of individual cell responses. Both the Pereira model and our experimental results are consistent with the "set-point" concept put forth by Frost more than two decades ago (50). He posited that the then-unknown mechanosensor in bone (now known to be the osteocyte) had a mechanical strain set-point for activation, analogous to the set-point of a thermostat. Once the mechanosensor, or "mechanostat," is turned on by the appropriate strain, it would signal actuator cells (osteoblasts or osteoclasts) to adapt bone.

A number of studies have examined osteocyte Ca^{2+} signaling in situ by using explanted bones (10, 17). Adachi et al. found that osteocytes in calvaria deformed by using a needle showed a rapid and prolonged increase of Ca^{2+} concentration (51). Jing et al. found that osteocytes in explanted mouse tibiae displayed repetitive Ca^{2+} spikes in response to cyclic loading, with spike frequency and magnitude dependent on load magnitude (10). They further reported that Ca^{2+} responses were dependent on purinergic signaling, consistent with the mechanism reported by Thi et al. for isolated osteocytes (16). Jing et al. found that Ca^{2+} peaks of mechanically loaded osteocytes in explants were of longer duration and at a much slower rate than the mechanical input stimulus (10). The results of our studies on osteocytes in vivo differ substantially. Why these differences occur is not yet clear, but contributing factors likely include removal of explant bone from its normal vascular environment, which will alter LCS fluid pressure (8, 18, 19), solute transport, and oxidative stresses on osteocytes (20). Indeed, in our study of in vivo vs. postmortem effects, we observed that osteocyte responses to mechanical loading change rapidly and markedly once vascular pressure is removed.

We report here information about real-time osteocyte Ca^{2+} responses in vivo. We found that number of osteocytes responding to load was strongly correlated to strain magnitude and that osteocyte load–response curves were also dependent upon loading frequency. These data indicate that tight coupling between loading and number of responding osteocytes is an essential feature of the control of bone mechanosensing and, ultimately, adaptation to mechanical loading. Indeed, having sensors or measurement systems that precisely track input is an indispensable feature of precision engineering controls systems. That osteocyte populations precisely track loading stimuli both in terms of magnitude and frequency also suggests parallels to sensory information encoding in the nervous system, where deviations from normal tightly coupled encoding behaviors are often typical of diseases. We speculate that hormonal or cell

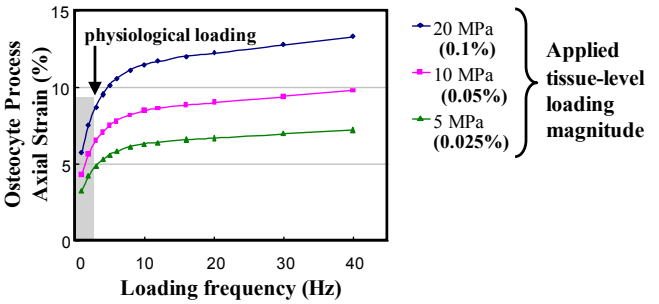

Fig. 6. Predicted axial strain at the transduction sites on the osteocyte process cell membrane as a function of loading frequency at various tissue-loading magnitudes [adapted from the mathematical model of Wang et al. (5)]. The shaded region has been added to highlight the exponential increases in focal membrane strains expected on osteocyte process over the physiological frequency range examined experimentally in the present studies.

alterations that disrupt the couplings between osteocyte recruitment and mechanical input may be characteristic or even predictive of skeletal diseases such as osteoporosis.

Materials and Methods

Details regarding device development and study methods can be found in *SI Materials and Methods*.

Mice Expressing Osteocyte-Targeted GCaMP3. Mice exhibiting osteocyte-targeted GCaMP3 (designated OtGP3) were obtained by mating Ai38 mice [B6;129S-Gt(ROSA)26Sortm38(CAG-GCaMP3)Hze/J; JAX Labs] with DMP1/Cre mice [B6N.FVB-Tg(Dmp1-cre)1Jqfe/BwdJ; JAX Labs], which possess Cre recombinase driven by a 10-kb fragment of the DMP1 promoter, which is dominantly expressed in osteocytes and odontoblasts (52). Mice were bred onto a C57BL/6 background. Studies used 16-wk-old female mice and all procedures were approved by the Institutional Animal Care and Use Committees at both Albert Einstein College of Medicine and City College of New York.

Structural and Material Properties of OtGP3 and B6 Metatarsal Bones. Structural and mineralization studies were performed by using micro-CT (μCT) to assess OtGP3 vs. WT C57Bl/6 bones as detailed elsewhere (53) (n = 6 bones per genotype). Lamellar vs. woven bone area and osteocyte density (number per mm^2) were measured at 400$\times$ magnification from 5-μm-thick middiaphyseal cross-sections, which were counterstained with toluidine blue.

In Vivo Mechanical Loading Apparatus. We created a mechanical loading device for in vivo three-point bending of MT3 during simultaneous multiphoton imaging (Ultima; Bruker Instruments) of osteocytes in vivo. Loading apparatus details (Fig. S2) and strain calibrations data (Fig. S3) are presented in *SI Materials and Methods*. Osteocytes were visualized in middiaphyses between upper loading contact points (tensile region). Loading studies were performed under displacement control.

Osteocyte Response to Mechanical Loading in Vivo. Under isoflurane anesthesia, the MT3 dorsal surface was accessed, and the foot was positioned in the loading apparatus. Isoflurane does not alter Ca^{2+} signaling (54). Bones were loaded cyclically to strain magnitudes of 250, 500, 1,000, 2,000, and 3,000 $\mu\epsilon$. Strains up to $\sim$2,000 $\mu\epsilon$ occur in diaphyses in vivo and are characteristic of normal physiological activities from moderate walking to running (55, 56). The highest strain level examined (3,000 $\mu\epsilon$) is typical of extreme activities and approximates the threshold reported for turning on periosteal woven bone apposition (38). Loading frequency effects were examined as well, with groups tested at 0.5, 1, or 2 Hz (n = 6 per frequency). Images were acquired in two ROIs located immediately on either side of the middiaphysis. These ROIs were chosen because they had effectively no measurable strain gradients based on strain calibration studies (see *SI Materials and Methods* for details). Images were collected continuously for a 60-s loading period at each test strain. The bone was then unloaded and allowed to rest for 15 min, which exceeds the refractory period for bone cells (57). This procedure was repeated for each strain level, going from lowest to highest strain at one imaging site and then from highest to lowest strain at the adjacent imaging site to assess potential conditioning or offset in osteocyte response from loading sequence. No sequential effect was observed. Mice were euthanized at the end of the loading study.

In addition, we used this experimental system to assess whether vascular pressure contributes to osteocyte response in vivo. MT3 from additional mice (n = 3 males) were loaded to a single test strain (2,000 $\mu\epsilon$), and osteocyte Ca^{2+} response was measured. Mice were then euthanized in place, and loading and imaging were repeated at 15 and 60 min after death; 60 min approximates incubation times reported in bone explant studies (10, 17, 58).

Imaging. Osteocyte Ca^{2+} response in MT3 bones of OtGP3 mice during whole bone loading was visualized by using MPM. By using a 40$\times$ magnification water immersion objective, imaging was performed with 920-nm wavelength excitation and 490- to 560-nm bandpass filter acquisition at 6 frames per second. Osteocytes were imaged in a single optical plane located $\sim$20 μm below the periosteal surface to maintain uniform strain distribution within the ROI. Ca^{2+} intensity measurements from osteocytes observed were performed by postprocessing images using ImageJ (NIH). Fluorescence intensity for each cell was normalized to its mean intensity for a 30-s period before the start of loading. GCaMP3 and other GECIs have a lower signal-to-noise ratio than exogenous Ca^{2+} sensing dyes (5 vs. 12, respectively), and, thus, a lower potential fold change in fluorescent intensity (59, 60). Accordingly, osteocytes were considered as responding if they exhibited $>$25% increase in normalized fluorescence intensity during loading.

Statistical Analyses. The μCT and histological difference between mouse strains were assessed by using the t test. Differences in osteocyte response vs. strain level among strain groups were examined by using either ANOVA with Fisher's least squared difference for post hoc testing or regression analyses. Analyses were performed with SPSS (Version 20; IBM).

ACKNOWLEDGMENTS. We thank Dr. Adrian Rodriguez-Contreras for assistance with multiphoton microscopy and Dr. Susanah Fritton for assistance with Fig. 6. This work supported by NIH Grants AR041210, AR057139, DK091466, and DK081435.

1. Cabahug-Zuckerman P, et al. (2016) Osteocyte apoptosis caused by Hindlimb unloading is required to trigger osteocyte RANKL production and subsequent resorption of cortical and Trabecular bone in mice femurs. *J Bone Miner Res* 31:1356–1365.
2. Plotkin LI, et al. (2015) Inhibition of osteocyte apoptosis prevents the increase in osteocytic receptor activator of nuclear factor κB ligand (RANKL) but does not stop bone resorption or the loss of bone induced by unloading. *J Biol Chem* 290:18934–18942.
3. Emerton KB, et al. (2010) Osteocyte apoptosis and control of bone resorption following ovariectomy in mice. *Bone* 46:577–583.
4. Kennedy OD, et al. (2012) Activation of resorption in fatigue-loaded bone involves both apoptosis and active pro-osteoclastogenic signaling by distinct osteocyte populations. *Bone* 50:1115–1122.
5. Wang Y, McNamara LM, Schaffler MB, Weinbaum S (2007) A model for the role of integrins in flow induced mechanotransduction in osteocytes. *Proc Natl Acad Sci USA* 104:15941–15946.
6. Bonewald LF, Johnson ML (2008) Osteocytes, mechanosensing and Wnt signaling. *Bone* 42:606–615.
7. Schaffler MB, Cheung WY, Majeska RJ, Kennedy O (2013) Osteocytes: Master orchestrators of bone. *Calcif Tissue Int* 94:5–24.
8. Fritton SP, Weinbaum S (2009) Fluid and solute transport in bone: Flow-induced mechanotransduction. *Annu Rev Fluid Mech* 41:347–374.
9. Verbruggen SW, Vaughan TJ, McNamara LM (2013) Fluid flow in the osteocyte mechanical environment: A fluid–structure interaction approach. *Biomech Model Mechanobiol* 13:85–97.
10. Jing D, et al. (2014) In situ intracellular calcium oscillations in osteocytes in intact mouse long bones under dynamic mechanical loading. *FASEB J* 28:1582–1592.
11. Klein-Nulend J, Bakker AD, Bacabac RG, Vatsa A, Weinbaum S (2012) Mechanosensation and transduction in osteocytes. *Bone* 54:182–190.
12. Lu XL, Huo B, Park M, Guo XE (2012) Calcium response in osteocytic networks under steady and oscillatory fluid flow. *Bone* 51:466–473.
13. Hung CT, Allen FD, Pollack SR, Brighton CT (1996) Intracellular Ca2+ stores and extracellular Ca2+ are required in the real-time Ca2+ response of bone cells experiencing fluid flow. *J Biomech* 29:1411–1417.
14. Ajubi NE, et al. (1996) Pulsating fluid flow increases prostaglandin production by cultured chicken osteocytes–a cytoskeleton-dependent process. *Biochem Biophys Res Commun* 225:62–68.
15. Bakker AD, Soejima K, Klein-Nulend J (2001) The production of nitric oxide and prostaglandin E 2 by primary bone cells is shear stress dependent. *J Biomech* 34:671–677.
16. Thi MM, Suadicani SO, Schaffler MB, Weinbaum S, Spray DC (2013) Mechanosensory responses of osteocytes to physiological forces occur along processes and not cell body and require $\alpha V\beta 3$ integrin. *Proc Natl Acad Sci USA* 110:21012–21017.
17. Hu M, Tian GW, Gibbons DE, Jiao J, Qin YX (2015) Dynamic fluid flow induced mechanobiological modulation of in situ osteocyte calcium oscillations. *Arch Biochem Biophys* 579:55–61.
18. Wang L, Fritton SP, Weinbaum S, Cowin SC (2003) On bone adaptation due to venous stasis. *J Biomech* 36:1439–1451.
19. Cowin SC, Cardoso L (2015) Blood and interstitial flow in the hierarchical pore space architecture of bone tissue. *J Biomech* 48:842–854.
20. Frikha-Benayed D, Basta-Pljakic J, Majeska RJ, Schaffler MB (2016) Regional differences in oxidative metabolism and mitochondrial activity among cortical bone osteocytes. *Bone* 90:15–22.
21. Huo B, Lu XL, Costa KD, Xu Q, Guo XE (2010) An ATP-dependent mechanism mediates intercellular calcium signaling in bone cell network under single cell nanoindentation. *Cell Calcium* 47:234–241.
22. Jing D, et al. (2013) Spatiotemporal properties of intracellular calcium signaling in osteocytic and osteoblastic cell networks under fluid flow. *Bone* 53:531–540.
23. Jacobs CR, Temiyasathit S, Castillo AB (2010) Osteocyte mechanobiology and pericellular mechanics. *Annu Rev Biomed Eng* 12:369–400.

24. Thi MM, Urban-Maldonado M, Spray DC, Suadicani SO (2010) Characterization of hTERT-immortalized osteoblast cell lines generated from wild-type and connexin43-null mouse calvaria. *Am J Physiol-Cell Physiol* 299:C994–C1006.
25. Zaman G, et al. (1999) Mechanical strain stimulates nitric oxide production by rapid activation of endothelial nitric oxide synthase in osteocytes. *J Bone Miner Res* 14:1123–1131.
26. Xu H, et al. (2012) Oscillatory fluid flow elicits changes in morphology, cytoskeleton and integrin-associated molecules in MLO-Y4 cells, but not in MC3T3-E1 cells. *Biol Res* 45:163–169.
27. Lu XL, Huo B, Chiang V, Guo XE (2012) Osteocytic network is more responsive in calcium signaling than osteoblastic network under fluid flow. *J Bone Miner Res* 27: 563–574.
28. Takai E, Mauck RL, Hung CT, Guo XE (2004) Osteocyte viability and regulation of osteoblast function in a 3D trabecular bone explant under dynamic hydrostatic pressure. *J Bone Miner Res* 19:1403–1410.
29. Kamel MA, Picconi JL, Lara-Castillo N, Johnson ML (2010) Activation of β-catenin signaling in MLO-Y4 osteocytic cells versus 2T3 osteoblastic cells by fluid flow shear stress and PGE2: Implications for the study of mechanosensation in bone. *Bone* 47:872–881.
30. Kitase Y, et al. (2010) Mechanical induction of PGE2 in osteocytes blocks glucocorticoid-induced apoptosis through both the β-catenin and PKA pathways. *J Bone Miner Res* 25:2657–2668.
31. Kramer I, et al. (2010) Osteocyte Wnt/-catenin signaling is required for normal bone homeostasis. *Mol Cell Biol* 30:3071–3085.
32. Bellido TM, et al. (2005) Chronic elevation of parathyroid hormone in mice reduces expression of sclerostin by osteocytes: A novel mechanism for hormonal control of osteoblastogenesis. *Endocrinology* 146:4577–4583.
33. Robling AG, et al. (2008) Mechanical stimulation of bone in vivo reduces osteocyte expression of Sost/sclerostin. *J Biol Chem* 283:5866–5875.
34. Gu X, Spitzer NC (1995) Distinct aspects of neuronal differentiation encoded by frequency of spontaneous Ca2+ transients. *Nature* 375:784–787.
35. Sharma D, et al. (2012) Alterations in the osteocyte lacunar–canalicular microenvironment due to estrogen deficiency. *Bone* 51:488–497.
36. Ciani C, Sharma D, Doty SB, Fritton SP (2014) Ovariectomy enhances mechanical load-induced solute transport around osteocytes in rat cancellous bone. *Bone* 59:229–234.
37. Forwood MR, Turner CH (1995) Skeletal adaptations to mechanical usage: Results from tibial loading studies in rats. *Bone* 17:197S–205S.
38. Turner CH, Forwood MR, Rho JY, Yoshikawa T (1994) Mechanical loading thresholds for lamellar and woven bone formation. *J Bone Miner Res* 9:87–97.
39. Hsieh YF, Turner CH (2001) Effects of loading frequency on mechanically induced bone formation. *J Bone Miner Res* 16:918–924.
40. Robling AG, Hinant FM, Burr DB, Turner CH (2002) Improved bone structure and strength after long-term mechanical loading is greatest if loading is separated into short bouts. *J Bone Miner Res* 17:1545–1554.
41. Forwood MR, Burr DB (1993) Physical activity and bone mass: Exercises in futility? *Bone Miner* 21:89–112.
42. Salvi JD, Maoiléidigh DÓ, Fabella BA (2015) Control of a hair bundle's mechanosensory function by its mechanical load. *Proc Natl Acad Sci USA* 112:E1000–E1009.
43. Dick IE, et al. (2008) A modular switch for spatial Ca2+ selectivity in the calmodulin regulation of CaV channels. *Nature* 451:830–834.
44. You L, Cowin SC, Schaffler MB, Weinbaum S (2001) A model for strain amplification in the actin cytoskeleton of osteocytes due to fluid drag on pericellular matrix. *J Biomech* 34:1375–1386.
45. Nawaz S, et al. (2012) Cell visco-elasticity measured with AFM and optical trapping at sub-micrometer deformations. *PLoS One* 7:e45297–e45299.
46. Skerry TM, Bitensky L, Chayen J, Lanyon LE (1989) Early strain-related changes in enzyme activity in osteocytes following bone loading in vivo. *J Bone Miner Res* 4: 783–788.
47. Inaoka T, et al. (1995) Sequential analysis of gene expression after an osteogenic stimulus: c-fos expression is induced in osteocytes. *Biochem Biophysical Res Commun* 217:264–270.
48. Rawlinson SC, Wheeler-Jones CP, Lanyon LE (2000) Arachidonic acid for loading induced prostacyclin and prostaglandin E(2) release from osteoblasts and osteocytes is derived from the activities of different forms of phospholipase A(2). *Bone* 27: 241–247.
49. Pereira AF, Javaheri B, Pitsillides AA, Shefelbine SJ (2015) Predicting cortical bone adaptation to axial loading in the mouse tibia. *J R Soc Interface* 12: 0590.
50. Frost HM (1983) A determinant of bone architecture. The minimum effective strain. *Clin Orthop Relat Res*®:286–292.
51. Adachi T, et al. (2009) Osteocyte calcium signaling response to bone matrix deformation. *J Biomech* 42:2507–2512.
52. Lu Y, et al. (2007) DMP1-targeted Cre expression in odontoblasts and osteocytes. *J Dental Res* 86:320–325.
53. Cheung WY, et al. (2016) Pannexin-1 and P2X7-receptor are required for apoptotic osteocytes in fatigued bone to trigger RANKL production in neighboring bystander osteocytes. *J Bone Miner Res* 31:890–899.
54. Kim YS, et al. (2016) Coupled activation of primary sensory neurons contributes to chronic pain. *Neuron* 91:1085–1096.
55. Burr DB, et al. (1996) In vivo measurement of human tibial strains during vigorous activity. *Bone* 18:405–410.
56. Rubin CT, Lanyon LE (1984) Dynamic strain similarity in vertebrates; an alternative to allometric limb bone scaling. *J Theor Biol* 107:321–327.
57. Donahue SW, Donahue HJ, Jacobs CR (2003) Osteoblastic cells have refractory periods for fluid-flow-induced intracellular calcium oscillations for short bouts of flow and display multiple low-magnitude oscillations during long-term flow. *J Biomech* 36: 35–43.
58. Ishihara Y, et al. (2013) Ex vivo real-time observation of Ca2+ signaling in living bone in response to shear stress applied on the bone surface. *Bone* 53:204–215.
59. Mank M, Griesbeck O (2008) Genetically encoded calcium indicators. *Chem Rev* 108:1550–1564.
60. Hagen BM, Boyman L, Kao JPY, Lederer WJ (2012) A comparative assessment of fluo Ca2+ indicators in rat ventricular myocytes. *Cell Calcium* 52:170–181.
61. Nakai J, Ohkura M, Imoto K (2001) A high signal-to-noise Ca2+ probe composed of a single green fluorescent protein. *Nat Biotechnol* 19:137–141.
62. Ohkura M, Matsuzaki M, Kasai H, Imoto K, Nakai J (2005) Genetically encoded bright Ca 2+probe applicable for dynamic Ca 2+imaging of dendritic spines. *Anal Chem* 77:5861–5869.
63. Tsien RY (2009) Indicators based on fluorescence resonance energy transfer (FRET). *Cold Spring Harb Protoc* 2009:pdb.top57.
64. Schriefer JL, et al. (2005) A comparison of mechanical properties derived from multiple skeletal sites in mice. *J Biomech* 38:467–475.
65. Chen TW, et al. (2013) Ultrasensitive fluorescent proteins for imaging neuronal activity. *Nature* 499:295–300.